nuclear fusion
IAEA

PAPER • OPEN ACCESS

The lithium systems of the IFMIF-DONES facility

To cite this article: F.S. Nitti *et al* 2025 *Nucl. Fusion* **65** 122004

OPEN ACCESS
IOP Publishing | International Atomic Energy Agency
Nuclear Fusion
Nucl. Fusion **65** (2025) 122004 (20pp)
https://doi.org/10.1088/1741-4326/adc284

The lithium systems of the IFMIF-DONES facility

F.S. Nitti[1,*], J. Maestre[2], T. Dezsi[3,4], S. Gordeev[5], N. Holstein[5], B. Brenneis[5], L. Buligins[6], J. Molla[7], A. Ibarra[2,7] and EUROfusion WPENS Team[a]

[1] ENEA Brasimone, Camugnano, Italy
[2] IFMIF-DONES España, Granada, Spain
[3] Centre for Energy Research (EK-CER), Budapest, Hungary
[4] C3D Engineering Consultant Ltd, Budapest, Hungary
[5] KIT, Karlsruhe, Germany
[6] Institute of Physics University of Latvia, Rïga, Latvia
[7] Ciemat, Av. Complutense, 40, 28040 Madrid, Spain

E-mail: francesco.nitti@enea.it

Received 11 October 2024, revised 20 February 2025
Accepted for publication 19 March 2025
Published 24 September 2025

Abstract

The International Fusion Materials Irradiation Facility-DEMO Oriented Neutron Source (IFMIF-DONES) is designed mainly to test and qualify materials for future fusion reactors by exposing them to a high energetic and intense neutron flux, and also to develop other scientific experiments using a fraction of the neutrons generated. The Lithium Systems (LSs) are crucial to the operation of the facility, generating and delivering the neutron flux through the interaction of a deuteron beam with a flowing lithium target. It comprises four systems: the Target System that produces the stable high-velocity lithium flow target and handles the substantial heat load from the beam interaction; the Heat Removal Loops, designed to supply the liquid lithium to the target in adequate conditions, this removing up to 10 MW through primary lithium loops and secondary and tertiary oil and water loops; the Impurity Control System, which controls the contents of impurities in the lithium, to reduce corrosion and erosion phenomena, and localize the radioactive impurities; and the LS Ancillaries, providing essential support such as vacuum, gas, and electrical power to the other systems. The design and operation of the LSs face several significant challenges. Maintaining the stability and high velocity of the lithium flow under extreme conditions is of paramount importance. Operating in a high-radiation environment presents additional complexities, requiring the development of specialized maintenance strategies in conjunction with remote handling technologies. The design of the IFMIF-DONES LS has evolved over the last years. This paper presents the current design status, highlighting the solutions implemented to address these challenges and to ensure the reliable and safe operation of the facility.

[a] See the Appendix in Ibarra *et al* (https://doi.org/10.1088/1741-4326/adb864) for the EUROfusion WPENS Team.
[*] Author to whom any correspondence should be addressed.

Keywords: IFMIF-DONES, neutron-source, lithium-loop, target, diagnostics

(Some figures may appear in colour only in the online journal)

1. Introduction

The characteristics of the neutron field typical of a fusion reactor differ from those in fission reactors, with an energy peak around 14 MeV. The validation of the materials for fusion applications is of paramount importance, and tests of various samples of different shapes and dimensions irradiated under an adequate neutron flux is needed, to study the changes in their mechanical properties when exposed to conditions similar to those inside fusion reactors. This particular neutron flux is generated by the interaction of a deuteron beam with a flowing lithium target. This is briefly the essence of the International Fusion Materials Irradiation Facility-DEMO Oriented Neutron Source (IFMIF-DONES), a neutron source facility for the qualification of materials to be used in the first Demonstration Fusion power plant [1–3].

The core of the facility, responsible for generating the lithium target and delivering the neutron flux, is called the Lithium Systems (LS). The main function of the LSs is to generate a flowing liquid lithium (LL) target for enabling $D^+ - Li$ stripping reaction and produce an adequate neutron flux ($5 \cdot 10^{14}$ neutrons$/cm^2 s$) to properly irradiate the test modules, which allocate the samples. In particular the LS has: to maintain a constant high-velocity and stable free surface flow of liquid lithium (Li) in front of the D^+ beam; to remove the high thermal power deposited in the Li jet by the beam (5 MW); and to remove and control impurities in the liquid Li.

The LS include four subsystems: the Target System (TSY), the Heat Removal Loops (HRL), the Impurity Control System (ICS) and the Lithium System Ancillaries (LSA), figure 1.

The TSY is devoted to generate the stable lithium target and the required neutron flux; the HRL is designed to provide a Li flow to the TSY and to transfer the heat generated to the plant general Heat Rejection System (HRS); the ICS is devoted to reduce the impurities content in the lithium; and the LSA includes the ancillaries systems (vacuum, gas, electric power) of the LS.

The design of the LS was driven by a high-availability oriented criteria by mean the RAMI (Reliability, Availability, Maintainability and Inspectability) analysis tool. Indeed, starting from the loss of functionality of the systems by means the Failure Mode and Effect Analysis (FMEA), the performance of the systems in terms of reliability and availability, taking into account the maintainability and inspectability, is investigated by the Reliability Block Diagram and the Phase Diagram. The results of the analysis, which considers a period of 171 days of normal operation followed by a short preventive maintenance (3 days) and another period of 171 days of normal operation followed by a long preventive maintenance (20 days), shows that the LS of DONES, with its current layout and the maintenance policy applied, can have an availability of 94.5% during 20 years of operation, which match the required availability target of 94% [4].

Particular attention is also given to the safety of lithium management, especially in the context of accident analysis, recovery, inertization, and fire extinguishing. The chemical reactivity and potential flammability of lithium are critical considerations for its safe handling, particularly in scenarios involving large lithium leaks. A dedicated experimental facility, LiFIRE, has been recently commissioned to conduct further research studies related to these latter topics in support of the definition of the final lithium fire protection requirements [5].

A reliable fire protection methodology is being developed and implemented in design phase with the purpose to reduce as much as possible the risk of fire in case of lithium leaks, and to minimize or to avoid potential consequences, such as the mobilization of toxic aerosols and radionuclides. A Defense-in-Depth strategy has been adopted to define a comprehensive set of passive and active measures for preventing, detecting and mitigating lithium leakages and fires. The adopted solution for a robust and reliable Fire Protection System is a combination of passive safety elements (e.g. metal catch pans or boxes, lithium recovery and draining systems) and active systems for extinguishing potential lithium fires that might occur over the lifetime of the facility [6].

This paper provides a comprehensive overview of the current design status of LS, including safety, RAMI and Remote Handling (RH) considerations, as well as some insights on R&D activities for particular components and technologies.

2. Target system

2.1. System description and configuration

The TSY is devoted to generate a stable lithium target and a neutron flux with defined characteristics to allow the irradiation of the materials samples located in the High Flux Test Module (HFTM) placed behind it. The neutrons are generated by the nuclear interactions, which take place inside the Target Vacuum Chamber, between an accelerated deuteron (D+) beam of 125 mA current and 40 MeV energy, provided by one linear accelerator under an angle of 9°, and a free-surface high-speed jet (15 m s^{-1}) of LL flowing in front of it, figure 2.

The TSY shall meet the following main functions: to produce and steadily maintain a LL jet with a suitable thickness (25 mm), width (260 mm) and flow velocity (15 m s^{-1}) to fully stop the 5 MW D+ beam inside the lithium layer; to accept the D+ beam and create the proper geometric and vacuum conditions for its interaction with the Li jet on a rectangular footprint

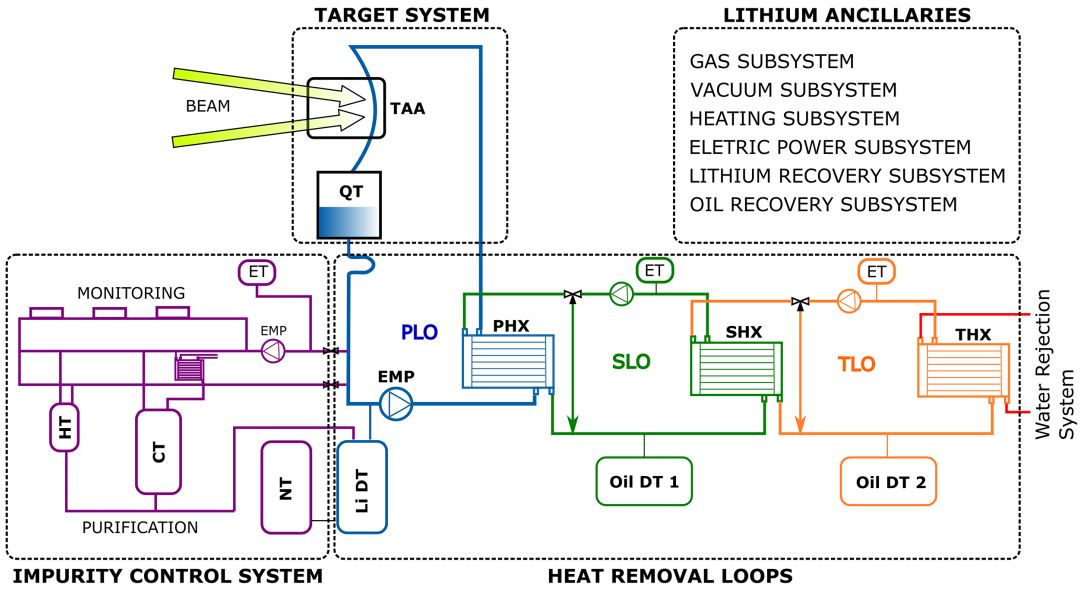

Figure 1. Schematic diagram of the LS.

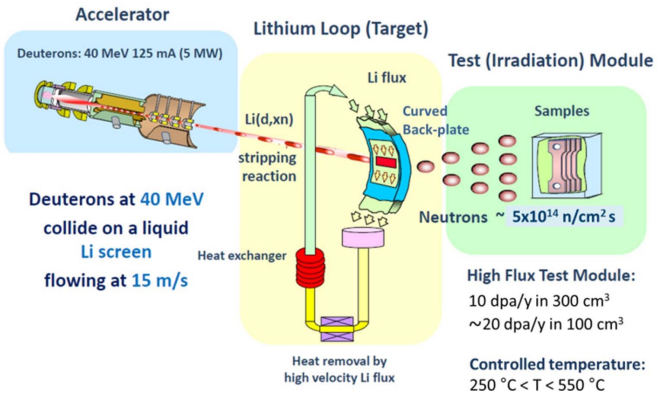

Figure 2. IFMIF-DONES facility schematic drawing.

area ranging from 10×5 cm^2 to 20×5 cm^2. Furthermore, the TSY is designed to be fully compatible not only with IFMIF-DONES, but also with its future upgrade, called simply IFMIF, where two 5 MW D+ beams are involved. For the current design, IFMIF-DONES load requirements have been used as the baseline to minimize potential impacts on system interfaces during future upgrades.

The TSY is located in an isolated and shielded room, called Test Cell (TC). Its main components are (see figure 3): Target Assembly (TAA), which includes: Inlet and Outlet Pipes, which routes the lithium from/to the main Li loop (outside the TC) to the TSY (inside the TC); Flow Straightener, which suppresses secondary flow and reduce turbulences in the Li flow; Reducer Nozzle, which accelerates the flow and generates the lithium jet; Backplate (BP), which hosts the concave channel [7], on which the high-speed lithium jet flows in front of the D+ beam; Quench Tank, which accepts the high-velocity free Li jet and converts it into a low-velocity confined flow; Vacuum Chamber, which creates and maintains the proper vacuum conditions for the interaction of the D+ beam with the Li jet; Beam Ducts, which connect the TSY with the accelerator line and the laser beam line for the Li jet diagnostics. The TAA is equipped with a tailored heating and insulation system. All the different components are equipped with independent heaters, except for the backplate, which cannot be obstructed to avoid disturbing the neutron flux. Therefore, the pre-heating of the TAA, to reach 200 °C in the BP, before the lithium circulation, is of fundamental importance to avoid potential solidification and plugging (Li melting temperature 180.5 °C). A pre-heating procedure has been numerically investigated and experimentally tested [8]. During the operation the heaters will control the temperatures of the components and balance the thermal losses. The flanges which use a fast connection system, for a RH manipulation, are not equipped with a heating and insulation system. Numerical investigation indicates that the thermal power lost by the flanges is negligible and the area of flanges connection is not a could point for the lithium, which is flowing at 6 m s^{-1} and 300 °C. The entire TSY operates under an intense radiation field that significantly challenges the limits of materials and devices. The backplate is the component most heavily exposed to the neutron flux, experiencing irradiation damage of approximately 20–30 dpa after one operational year (345 days) for a nominal beam (20×5 cm^2). As a result, its lifetime is expected to be limited, requiring periodic replacements. A preliminary assessment of the backplate lifetime, based on available material property data, indicates that irradiation embrittlement of its structural material (EUROFER-97) is the most critical issue. This assessment shows that the backplate may withstand one full operation year, though there are still some uncertainties due to the lack of material data under such fusion-like irradiation conditions. The primarily reason is the increase in its Ductile-to-Brittle Transition Temperature (DBTT) due to irradiation damage and helium production in

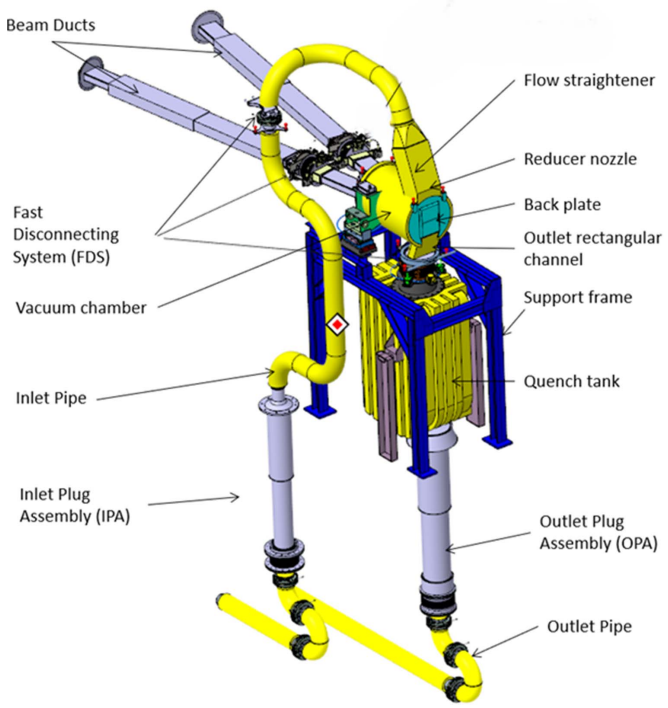

Figure 3. Target System schematic drawing. Reproduced from [3]. CC BY 4.0.

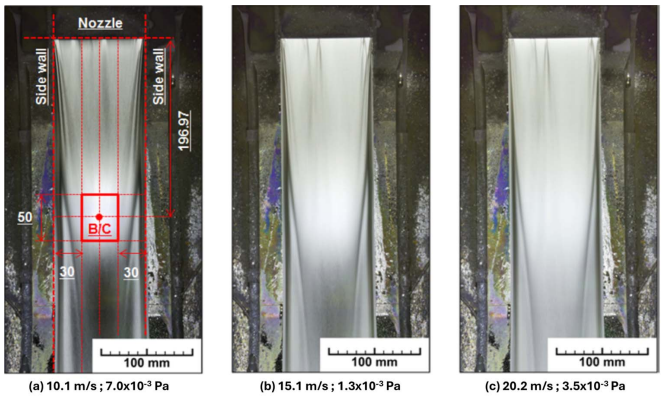

Figure 4. Appearance of Li target at different velocities. The jet width is 100 mm (1/2.6 of the nominal). In (*a*) the scaled beam footprint is shown. The beam center (B-C) is 196.97 mm vertical distance from the nozzle, the height of the beam foot print is 50 mm, and 30 mm is the distance from each side wall. Reprinted from [11], Copyright (2015), with permission from Elsevier.

the material as result of its exposition to the intense fusion-like neutron flux. The estimated lifetime of the BP comes from the time required to reach a DBTT close to the target operating conditions (250 °C–300 °C), this leading to a potential brittle failure. Furthermore, still based on currently available data obtained in non-fusion spectra, no swelling phenomena are expected to be observed due to the low operating temperature of the backplate compared to the onset swelling temperature which, for ferritic-martensitic steels (like EUROFER) has been observed to be >350 °C in the damage dose range of interest. However, these assumptions have an intrinsic uncertainty due to the lack of data in relevant environment and filling this gap is the main scope of the IFMIF-DONES project. On the other side, not any type of direct monitoring sensors of the back plate is foreseen due to the extreme radiation conditions and the difficulty of positioning the reliable diagnostics on that tight region. Therefore, this requires an annual replacement strategy of the target to ensure the proper operation of the facility during its lifetime.

Two different design configurations have been considered for the Target. The first one is an integral version, which is a fully welded solution where the entire Target Assembly (TAA) must be replaced as a single unit. Alternatively, a removable backplate concept, known as the Bayonet Concept, was developed [9]. In this design, the BP is connected to the fixed part (the target vacuum chamber) via a mechanism with a sealing flange, allowing only the BP to be replaced. While the Bayonet Concept offers several advantages, such as reducing the amount of activated material to be disposed of and simplifying target refurbishment operations, it also presents some technological challenges. These are primarily related to the performance and lifespan of the sealing mechanism, which is exposed to high irradiation doses that may degrade the seal and potentially lead to failure. Long-term exposure tests are being prepared to assess the seal's lifespan, though these tests are not fully representative of actual IFMIF-DONES conditions. In the current design, the baseline approach involves the annual replacement of the entire Target Assembly, including the vacuum chamber, straightener, nozzle, backplate, and disconnection systems (gaskets included).

In the period 2010–2015, in the framework of an Engineering Validation and Engineering Design Activity [10], called IFMIF-EVEDA phase, a Lithium Loop facility, ELTL (EVEDA Lithium Test Loop), was constructed and operated in Oarai, Japan, including a 1:2.6 scale target [11]. The hydrodynamic stability of the lithium jet was successfully validated over extended operational periods (1300 h) and reaching up to 20 m s^{-1} jet speed (see figure 4). The design of the TSY has progressed, focused on the integration within the TC, and paying particular attention to the replacement and maintenance developments via RH, as well as the integration of diagnostics. This includes also optimization of the quench tank and the design of advance supporting, installation and alignment features. Those developments are shown in following sections.

2.2. *Thermo-hydrodynamic and mechanic analysis*

Several thermal-hydraulic simulations have been developed to study the behavior of the lithium flowing in the nozzle, backplate and quench tank, both in startup phase and normal operation [12, 13]. The last update is related to a transient thermal-hydraulic simulations for the beam-on considering the lithium inlet temperature of 300 °C. As it is commented along this paper, a major design modification were recently

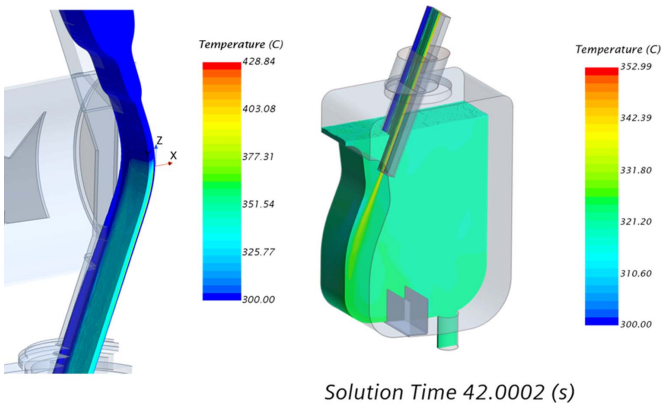

Figure 5. Temperature distribution in lithium jet and in quench tank.

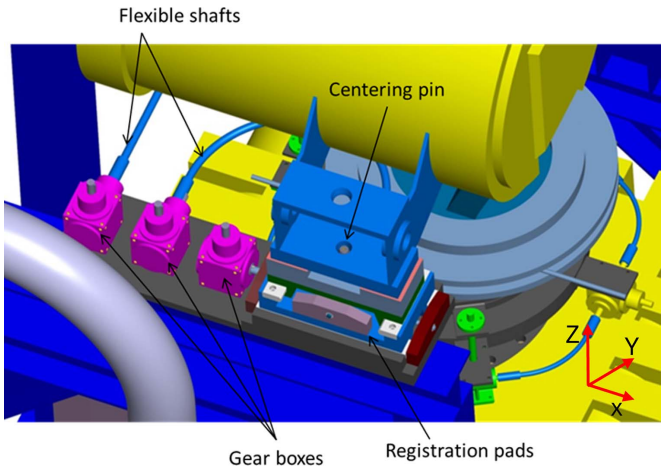

Figure 6. Target Assembly centering system.

implemented related with the increase of the nominal temperature from 250 °C to 300 °C in order to control the radioactive inventory in the lithium loop. This modifications implied the re-analysis of the TSY design. Figure 5 shows the temperature field in the lithium jet and QT. The lithium temperature field reaches its steady state in about 30 seconds. After, the warm and cold amounts of lithium in the QT are well mixed and the lithium temperature at the outlet reaches the saturation value of 318 °C.

Numerical analyses have been conducted to assess the thermo-mechanical behavior of the TSY under the steady-state nominal operating scenario. The goal was to verify whether its components can safely withstand the thermo-mechanical loads without experiencing significant deformations. Such deformations could warp the lithium channel, induce flow instability, interfere with the High Flux Test Module (HFTM), or cause misalignment between the deuteron beam and the lithium channel. The results showed that none of the cited problems are expected [14, 15].

2.3. Target assembly support

The target assembly support plays a crucial role with two main functions

- Sustains the TAA weight and counteracts the loading transferred to it by the TAA during normal operations and abnormal conditions (e.g. seismic events)
- Position the TAA and keep it aligned with respect to the D+ beam within the requested tolerances.

The support frame is a stainless steel (316 L) structure, equipped with four legs bolted to the TC floor at its bottom. The upper part of the support integrates the TAA centering and positioning system. Figure 6 provides a detailed view of these systems consisting of two registration pads (one for each TAA arm) and three sets of gearbox mechanisms for each TAA arm. The design aims to allow for the installation of the TAA to be completely remote-controlled.

The centering system uses a Pin-to-Hole and Pin-to-Slot concept, creating an isostatic arrangement for the TAA. The registration pads can slide independently in orthogonal directions, enabling fine adjustments of the TAA on the (X, Y) plane after centering. These pads slide on ceramic inserts to reduce friction and wear on the contact surfaces. Adjusting the TAA position involves moving the registration pads on which the centering pins are mounted. This movement is facilitated by gearboxes and flexible shafts, forming a one point manipulator system. Three gearboxes are utilized, providing three degrees of freedom, translations on the plane, and rotation outside the plane. This design allows the TAA to thermally expand in the three directions, preventing stresses from over-constraining the structure.

The centering pins design incorporates feedback from RH installation tests of the IFMIF TAA prototype performed at the ENEA (Italian National Agency for New Technologies, Energy and Sustainable Economic Development) laboratory. The gear boxes are also implemented in the Fast Disconnecting System (FDS) to expand and compress the bellows on the Beam Ducts.

2.4. Remote handling strategy

All maintenance operations to be performed on the TSY must be done through RH technologies as the TC environment is not accessible even during beam-off conditions due to high residual doses. The main operations to be carried out in the TC during the yearly scheduled maintenance period are [15]:

- The opening and closing of the TC.
- The plugging/unplugging of diagnostic and power electric connectors.
- The disconnection and connection of the FDS to disassemble the flanges.
- The exchange of TAA and its transportation to the Irradiated Material Treatment Cells for dismantling and waste conditioning.

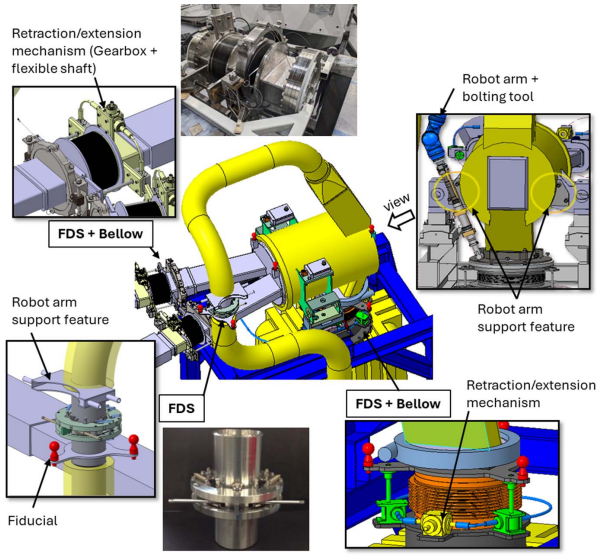

Figure 7. RH features for the connection of the TSY with lithium pipe, QT and beam ducts (FDS).

- The cleaning of the flanges, using a special tool already designed, manufactured and successfully tested.
- The installation of TAA and the link to the HFTM.
- The alignment of the TAA [16] and acceptance tests.

A series of features has been developed to allow and enhance previous operations. It is worth mentioning the FDS, which connects the target with the beam ducts, the QT and the lithium pipe. Main challenges are related to the harsh working conditions, under a strong irradiation field and in contact with lithium. They include an energized-type seal that ensures the leak-tightness, and the flanges are operated by RH tools. These components have been successfully prototyped (figure 7).

In addition, to perform these operations, a number of dedicated RH auxiliary devices and tools are foreseen. The main ones are:

- The heavy rope overhead crane covering the TC area. It consists on a multi-rope double beam overhead traveling crane dedicated to perform transfer operations of components with weights up to 140 Tons.
- The Access Cell Mast Crane (ACMC) which is a double beam overhead crane with a telescopic mast equipped with a change gripping system to allow connection with various devices and end-effectors. This device includes a series of tools, such as a Parallel Kinematic Manipulator (PKM); which allows the precise movements of heavy components inside the TC; and the robotic arm, equipped with seven degrees of freedom and designed to perform complex tasks in tight spaces as flange disconnection.

Figure 8 shows an illustration during the installation of the TAA on the Target Assembly Support by using the ACMC together with the PKM. The PKM facilitates precise positioning of the TAA by balancing gravity forces.

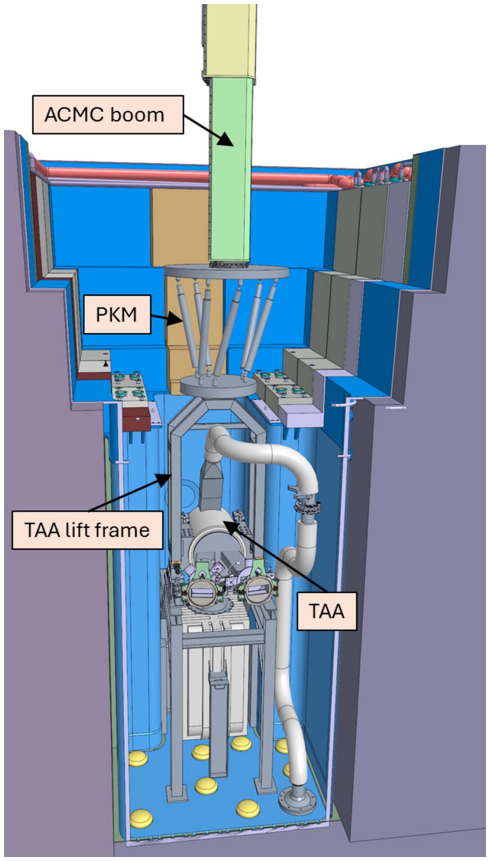

Figure 8. Illustrative 3D model of TAA positioning inside the Test Cell.

3. Heat removal loops

3.1. System description and configuration

The HRL is designed to provide lithium at constant flow rate and temperature to the TSY inlet; and to evacuate the heat deposition in the target (up to 10 MW, in case of the future planned expansion to two accelerator lines). The HRL comprises the Primary Loop (PLO), which recirculates the lithium between the TSY and the Primary Heat Exchanger (HX1); and the Secondary (SLO) and the Tertiary (TLO) oil loops that transfer the heat to the plant HRS, figure 9.

The PLO is designed to generate and control the lithium flow rate. The lithium is circulated by an electro-magnetic pump (EMP), throughout the HX1, to remove the thermal power deposited during the beam-target interaction. The HX1 transfers the heat from the lithium fluid, circulating into the shell side, to the oil stream that flows into the tube side. This heat is rejected to the water HRS by a series of two oil loops.

After conditioning, the Li flows across the Target Assembly to generate the Li jet at a constant flow rate and temperature. At the exit of the TAA the Li stream is collected in the quench tank where its velocity and temperature profile are uniformized before entering again in the EMP. Downstream the QT, two branch lines connect the primary loop to the ICS,

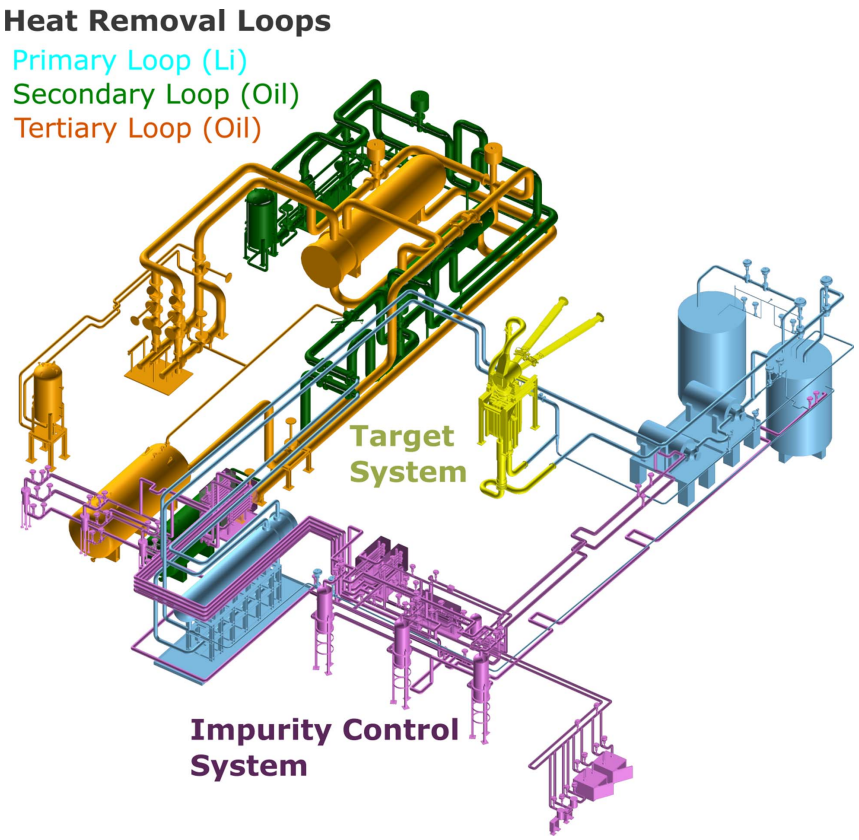

Figure 9. Illustrative 3D model of the Lithium Systems.

this being responsible of controlling the purity of the lithium. About 2% of the Li flow is extracted by a dedicated electromagnetic pump and re-injected into the primary loop.

Connected to the Li loop, a Dump Tank (DT) is provided to perform the lithium melting and accommodate the lithium during the first filling and system maintenance operations. An Argon Supply subsystem fills the DT with Ar at adequate pressure to support the charging and draining of Li in the loop.

The main design requirements and the sizing parameters of the PLO are summarized in table 1. The total amount of lithium, including the ICS, is 12.50 m^3. The pressure drop calculated in the PLO at nominal condition is 4 bar. Due to safety reasons, the loop is designed to be drained by gravity, further studies are ongoing to investigate the aid of injection of gas to improve the draining operation in case of emergency stop. The PLO is installed and confined in a dedicated room.

The Secondary and Tertiary loops have been designed to remove the thermal power gained by the Lithium flow through oil-oil (HX2) and oil-water (HX3) heat exchangers [17]. The SLO circulates organic oil forced by a centrifugal pump. The oil type, Dowtherm HT, is appropriately selected to have a boiling point over the maximum Li temperature reached in conditions of oil stop flowing into the HX1. The oil is heated on the tube side of the HX1 and cooled down on the tube side of the HX2. An expansion tank is provided to compensate the oil change volume in the loop and the pressure system fluctuations. A DT is provided to collect the oil during the system maintenance operations. See figure 1.

Similarly the TLO circulate oil, Dowtherm Q, forced by a centrifugal pump, which is heated on the shell side of the HX2 and cooled down on the tube side of the HX3. The water circulated in the shell side of the HX3 transfer the heat to the HRS. The SLO and TLO interface with the Argon Supply system to fill the Dump and Expansion tanks with Ar gas at a pressure slightly higher than 1 bar (abs.).

The thermal design parameters for the heat exchangers (HXs) at the nominal thermal power of 5 MW are detailed in table 2. These HXs are over-designed to meet requirements in case of an upgrade to IFMIF operation, which involves two deuteron beams with a total power of 10 MW. The basic design assumptions for the HXs is based on the TEMA standard [18], with an AEU (U-tube) type and TEMA class B. The materials used are A316L stainless steel. A minimum fluid velocity above 0.9 $m\,s^{-1}$ was considered in the design, as well as an additional thermal resistance due to fouling phenomenon. Additionally, a 30% over-sizing factor (safety factor) is applied for the heat transfer area. Each heat exchanger is equipped with temperature and pressure sensors at each inlet and outlet, 3-way globe valves to control the flow rate and regulate temperature, isolation valves on pipes penetrating walls with safety barrier requirements, and electrical heaters for additional temperature control.

The selected oil for HX1 has been studied within an experimental campaign to verify the variation of chemical-physical properties under irradiation. Note that the lithium may bring radioactive impurities, such as Beryllium-7, that may alter the

Table 1. Main design requirements of PLO.

ITEM	VALUE	NOTE
Constant Flow rate	97.5 l s^{-1}	Nominal value in the main Li loop
Li temperature in the cold leg of the loop	300 °C	at the exit of HX1
Heat removal capacity	5 MW	+30% margin for HX (extendable up to 10MW)
Component Material	SS316L	
Erosion/corrosion rate	$\leqslant$50 μm in 30 years	
Availability	>0.94	To fulfil the required LS availability 0.94, in scheduled operation time
Replacement period	30 years	

Table 2. Thermal design parameters for Heat Exchangers.

	Units	HX1	HX2	HX3
Shell side medium	—	Lithium	Dowtherm-Q	Water
Tube side medium	—	Dowtherm-HT	Dowtherm-HT	Dowtherm-Q
Shell side inlet temp.	°C	318	60	28.8
Shell side outlet temp.	°C	300	85	38.8
Tube side inlet temp.	°C	185	220	85
Tube side outlet temp.	°C	220	185	60
Shell side mass flow	kg s^{-1}	49.7	230	239
Tube side mass flow	kg s^{-1}	130	130	230
LMDT	°C	67.2	129.9	28.7

oil. The test showed a good chemical stability up to 13 MGy. The infrared analyses and the determination of the total acidity in the irradiated samples did not show appreciable changes compared to the non-irradiated oil. However, an increase in viscosity related to the adsorbed dose has been detected, which can be explained by the formation of higher molecular weight compounds by polymerization. A numerical simulation to estimate the dose rate in the oil in the HX1 during operation has shown a low level of radiation, highest dose rate around 0.003 Gy hr^{-1}, which confirm the suitability of the selected oil. Neutron streaming irradiation in the HX1, coming from the TAA, is negligible.

The SLO and TLO are installed and confined in a dedicated room separated from the PLO. A preliminary study is assessed in terms of loss of functionality for each component of the PLO. The FMEA at component level methodology has been applied for the purpose. Several different Postulate Initiating Events (PoIEs) have been outlined, as summarized in table 3, to be deeply analyzed by deterministic calculations in the next phases of the design.

3.2. Electromagnetic pump design and performance

Electromagnetic induction pumps are widely used for transporting liquid metals [20]. The main advantage of these pumps over mechanical pumps is the absence of moving parts submerged in the liquid metal, which eliminates seal problems. Their operation principle is based on the interaction between a traveling magnetic field and the currents induced by this field. This idea was first proposed by Einstein and Szilard in their 1930 patent [21], using three-phase inductor coils to create the linear traveling magnetic field. Recent advances in the production of permanent magnets have enabled the development of permanent magnet pumps (PMP). These pumps use rotating permanent magnetic poles with alternating polarity (figure 10) [22].

There are several main advantages of the PMP in comparison with the linear induction pumps: no energy is necessary for the creation of the magnetic field; the design is simpler because there is not winding in the pump, thus there is not risk of overheating and damaging of the electrical isolation of the winding; and the pump is usually more compact and light.

The PMP can be operated by a standard AC motors with the power supplied through a standard frequency converter, allowing to adjust the pump performance by adjusting rotation speed of the motor. The industrial motors and their frequency inverters are widely available, relatively cheap, well optimized and operate with high efficiency. In addition, a unique feature of PMPs is the ability to control the loop-pump system's inertia by modifying the rotor's moment of inertia, this determining the coast-down characteristic. However, a drawback of PMPs is the presence of moving parts, which require maintenance, such as bearings. Despite this, the maintenance procedures are well-established and cost-efficient. Moreover, the permanent magnets are in general sensitive to irradiation. However, the EMP is located in the Lithium Loop Cell and it

Table 3. List of PoIEs identified by the FMEA for the design of the PLO [4, 19].

PoIE	Postulated Initiating Event related to PLO
LS2-1	Loss of flow in the lithium loop because electro-magnetic pumps (EMPs) trip due to CCF
LS3-1	Loss of lithium in lithium loop area due to large break at the EMPs outlet
LS3-2	Loss of lithium in the TTC due to large break in piping running inside the cell
ORE	Increase of occupational radiation exposure due to operating the facility with abnormal operating conditions and/or to provide maintenance for decontaminations and repairing activities (This PoIE is identified for events not related to accident sequences that could impair containments and could lead to environmental release)
N/S	Not Safety Relevant

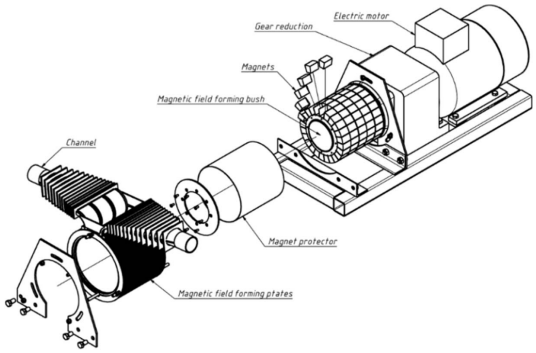

Figure 10. Exploded view drawing of a cylindrical type PMP.

is not exposed to neutrons. It may be exposed to the radiation coming from the impurities in the Lithium (mostly gamma at very low dose), which should have a negligible effect. The IFMIF-DONES PLO pump must meet several key requirements: the ability to deliver a nominal flow rate of 100 $\mathrm{l\,s^{-1}}$ with a pressure differential of 4 bars, operate under reduced suction pressure ($\sim$0.3 bar), and ensure high reliability and availability. Additionally, it must offer a long coast-down time (several seconds), a critical feature to ensure the lithium layer remains sufficiently present across the target, allowing for a beam stop in the event of pump trip or failure. Those requirements led to the selection of a PMP driven by a 160 kW AC motor, featuring a flywheel coupled to the motor axle.

The design of PMP has evolved during the last years. Especial focus has been paid to the EMP channel design and optimization of its magnetohydrodynamics performance. Analytical methods [20] and numerical simulations using COMSOL software have been widely used. Both approaches have been previously tested on a similar design pump, already available, and working with Na [23]. To fulfill the nominal flow rate for IFMIF-DONES, the cross-section of the available prototype pump has been increased from 3 to 5 subchannels, to increase the flow rate from 60 $\mathrm{l\,s^{-1}}$ to 100 $\mathrm{l\,s^{-1}}$. In addition, perforated inner walls are created to ensure more optimal induced current closing conditions, figure 11 [24].

Electrical potential formulation is used with insulating boundary conditions on outer walls and setting zero potential in the inlet and outlet boundary walls of the channel. The geometry of the magnetic rotor with air gap above it, where the Li channel is located, and the mesh for calculations is shown in figure 12 left. Perfect magnetic conductor boundary conditions are applied on inner and outer radial surfaces and magnetic insulation boundary conditions are applied on both sides (z axis). Magnetization of permanent magnets is set up according to Halbach array using remanent flux density $B_{\mathrm{rem}} = 1.1$ T according to Sm_2Co_{17} magnets. The partly assembled rotor is shown in figure 12 right.

Calculated magnetic field flux density and lines are shown in x-y plane (figure 13 top) and are essentially constant over z axis. Distribution of magnetic field in the air gap (figure 13 bottom) is exported and is used in the calculations for induced currents and heat in channel walls and for MHD calculation in liquid metal layer.

$k-\varepsilon$ turbulence model is used for Li flow and zero pressure condition is set in the outlet of the channel. Calculated eddy currents and velocity magnitude,related to a rotational speed of the rotor $n = 425$ rpm, are shown in figure 14. Area averaged pressure of all 5 sub-channels is used in the results. Obtained results of developed averaged pressure in figure 15 show that 4 bars with flowrate 100 $\mathrm{l\,s^{-1}}$ and operating temperature 350 °C

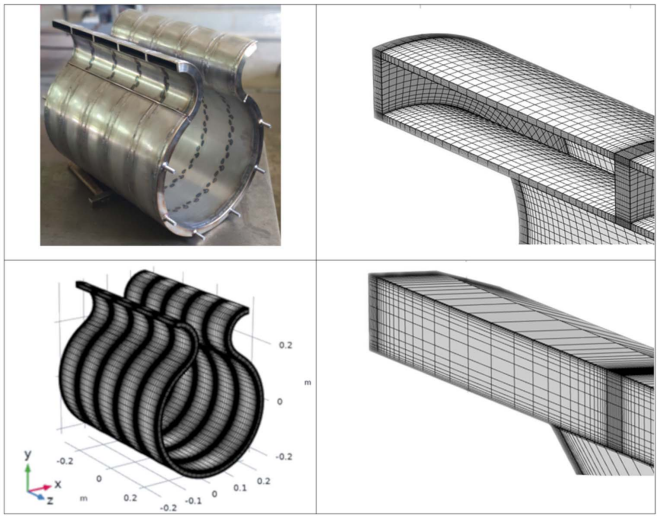

Figure 11. Left—PMP channel with 5 subchannels and overall mesh used for flow calculation—right—zoom in of meshes for magnetic field and hydrodynamics, 1926 600 and 363 636 elements correspondingly.

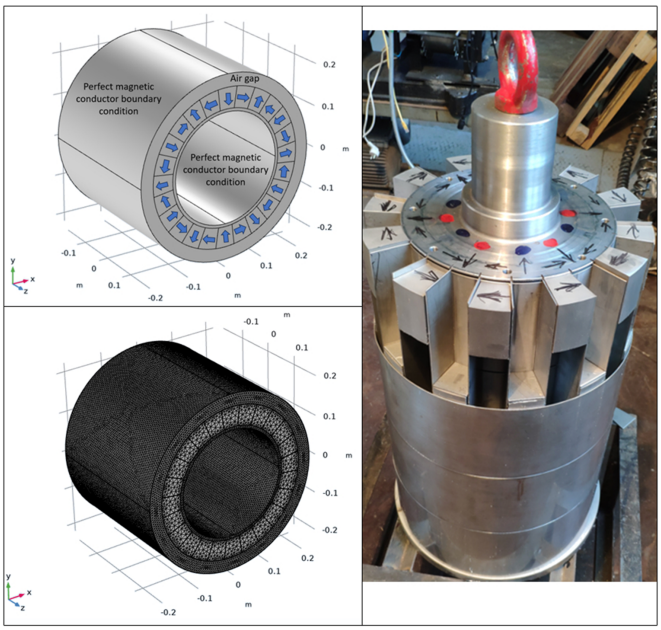

Figure 12. The geometry for calculation of magnetic field and mesh for calculation of magnetic field, size: 1575 379 elements (left). Right—rotor in assembling process. Arrows indicate direction of magnetization.

will be achieved at approximately 416 rpm, which is consistent with value obtained by analytical methods.

As previously mentioned, one of the design requirements is the ability to maintain half of the lithium flow rate, at least, through the target for several seconds (enough time to stop the beam) in the event of a pump failure. To address this, coast-down experiments have been conducted to demonstrate the possibility of significantly increasing coast-down times. PMPs with attached flywheels, each with four different values of rotational inertia, were used in the experiments, as shown in figure 16.

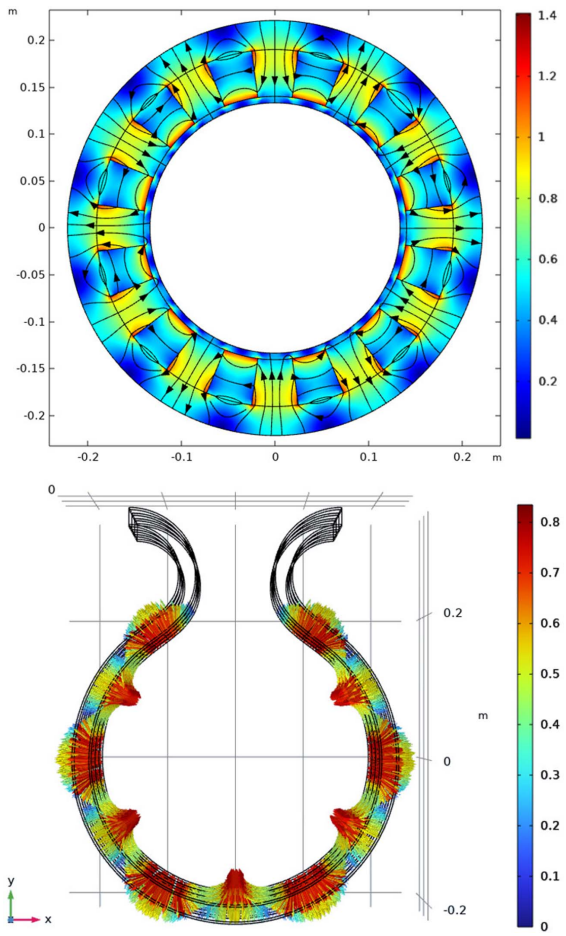

Figure 13. Top—calculated magnetic field; Bottom—applied external magnetic field in channel (both in (*T*).

Experimental results are compared with predictions of developed mathematical model which describes rotational movement of rotor with good agreement, figure 17. The power data [23] have been used for determination of the decay times. It is shown, that pump's rotor dynamics is well suited for flow rate dynamics characterization. This strategy is demonstrated to be efficient and fulfill the design requirements.

4. Impurity control system

4.1. System description and configuration

The ICS plays a crucial role for the reliable and safety operation of the LS. During operation, different kind of impurities are generated and distributed in the lithium loop. They are non-metallic impurities such as, Oxygen (O), Nitrogen (N), Hydrogen (H) and Carbon (C); and metallic impurities. The metallic impurities come mostly from metallic components and pipes (AISI 316 L and Eurofer-97) due to the corrosion and erosion phenomenon exerted by lithium. Actually, the corrosion-erosion phenomena may be enhanced by the presence of non-metallic impurities, mainly nitrogen, producing different compounds. Additionally, some other elements are generated as a result of the Li-beam interaction when passing

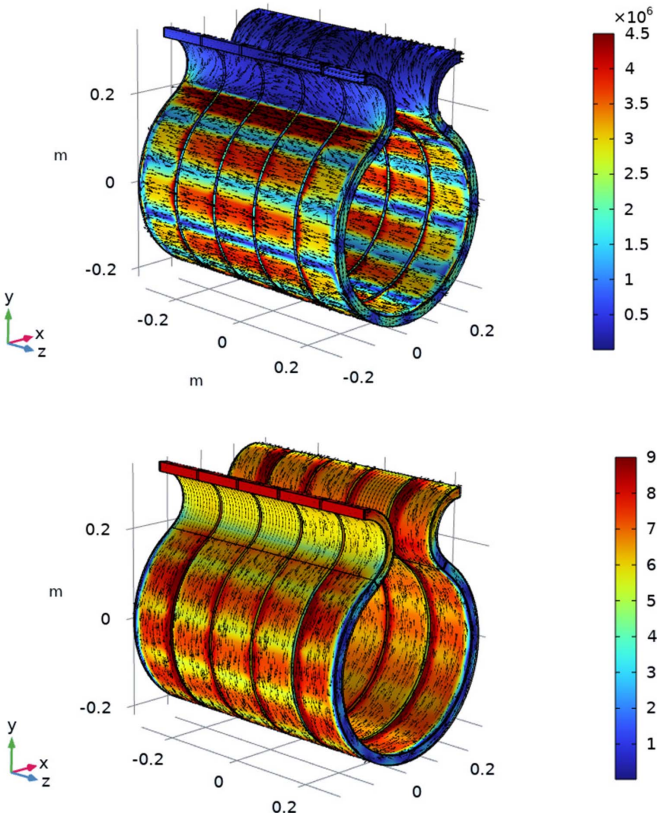

Figure 14. Eddy currents (A m^{-2}), Top, and Li velocity (m s^{-1}), Bottom.

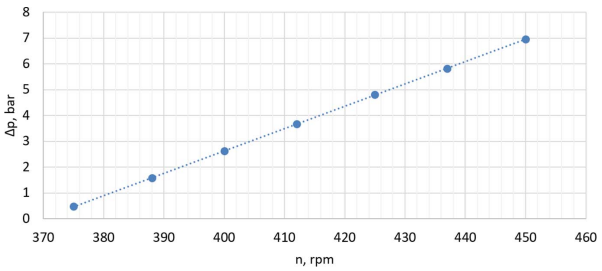

Figure 15. Developed pressure for 350 °C Li at $Q = 100$ l s^{-1} as function of magnetic field rotation speed.

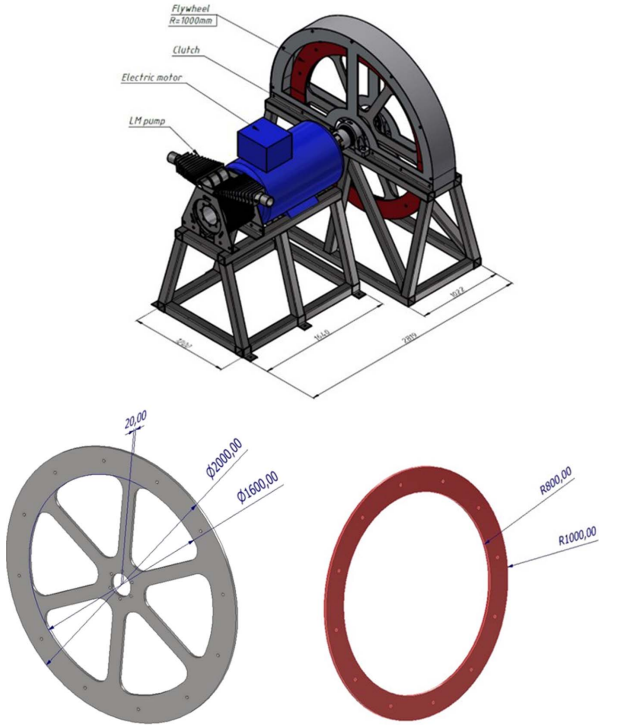

Figure 16. Overall view of PMP with flywheel, flywheel and ring.

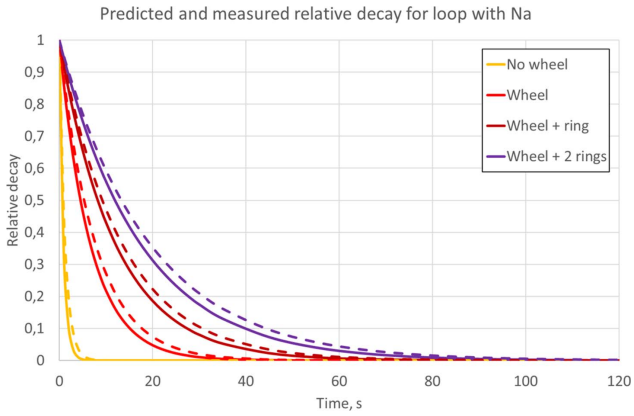

Figure 17. Predicted and measured time dependence of normalized rotor's angular speed. Solid line—experiment, dashed—theory.

through the TSY such as beryllium-7 (^{7}Be), tritium (T), and Activated Corrosion Product (ACP) due to the nuclear transmutations of the Corrosion Products (CPs) generated in the loop. The ICS is designed to both: control impurity levels of the sources of the corrosion and erosion on structural components (H, O, N, C); and confine or localize the sources of radioactivity such as T, ^{7}Be and ACPs.

Figure 18 shows an illustration of the ICS. It is conceived as a sub-loop bypassing the main loop, connected just upstream of the main EMP. It is divided in two sub-loops or branches: the purification and the monitoring. ICS contains a dedicated pump to drive the lithium through it. An expansion tank is located at the suction point that ensures enough head to avoid cavitation. The main design requirements and operational parameters are summarized in table 4.

The ICS is equipped with three types of traps that aim to capture the different impurities. Depending on the trapping and working principles, those are: Cold-trap (CT); Hydrogen-trap (HT) and Nitrogen-trap (NT). The first two traps operate continuously (in-line) and are installed in the purification branch, whereas the NT works off-line, only when the loop is stopped, and it is connected to the main DT.

The cold trap (CT) operates on the principles of temperature-dependent solubility and precipitation. Operating at a temperature, minimum 190 °C, near lithium's solidification point (180.5 °C), it efficiently captures lithium oxides, carbides, nitrides, hydrides, CPs, ACPs, and beryllium nitrides, depending on their solubility. A stainless steel mesh, hosted into a vessel, provides the surface to promote crystallization and precipitation of the impurities.

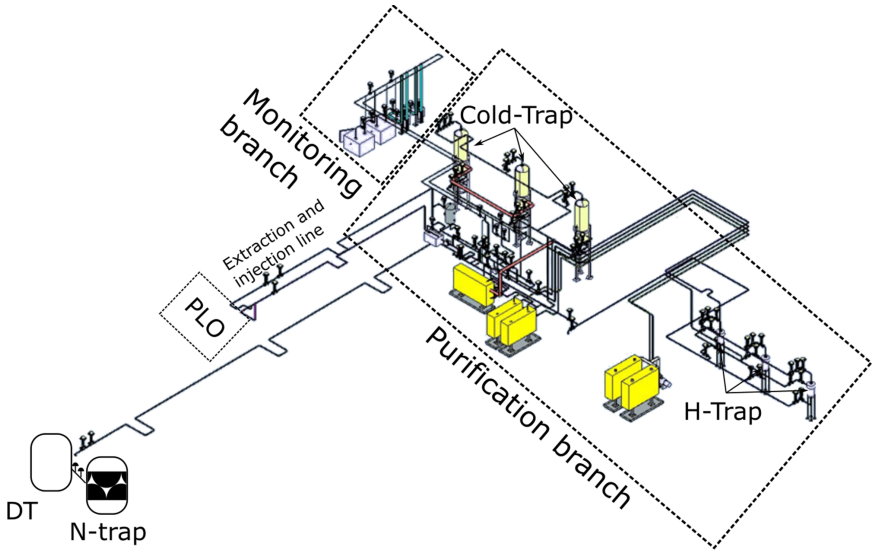

Figure 18. Overall view of the Impurity Control System.

Table 4. Main design requirements of ICS.

Item	Value	Notes
Flow rate	2.015 l s^{-1}	Purification branch = 1.95 l s^{-1}; Monitoring branch = 0.065 l s^{-1}
Li temperature	190–600 °C	Range of temperature (including the traps)
H content in Li	⩽10 wppm	target values, TBC
T quantity	0.3 g (in both Lithium and Yttrium system)	
N content in Li	⩽30 wppm	
O content in Li	⩽10 wppm	
Be-7 content in Li	(-)	No deposition outside Cold trap
Component material	SS316L	For piping system and equipment, except for traps
Availability	0.94	in scheduled operation time
Replacement period	Monthly	For H-trap
	30 years	In general, for the ICS
Replaceability	Possible	for all

The cooling process is made in two-step: lithium is first cooled using an economizer, then further cooled down with a lithium-diathermic oil heat exchanger (hairpin type). This setup optimizes thermal energy flow and ensures gradual cooling.

The design includes three vertical cylindrical CT tanks (≈1150 dm^3) in parallel, each filled with stainless steel mesh sheets (∼ 360×mesh:41.1, wire diameter 0.24 mm, sieve opening 0.38 mm, open surface 37.9%). This configuration offers certain operational flexibility, allowing two tanks to operate whilst the third one may be under maintenance. This ensures a residence time of 18 minutes for lithium, enough for efficient impurity capture based on previous experiences [25–29].

It should be noted that rapid cooling of Li directly to the lowest temperature of the CT (190 ° C) may produce blocking due to the prompt precipitation of impurities at the inlet. The so-called plugging-meter, utilized in sodium loops, may be used to control the precipitation temperature by measuring the flow rate drop through a thin orifice system in a cooled bypass pipe [30]. This device can be used to precisely regulate operating temperature of the CT, enabling gradual cooling and preventing blockages. Additionally, the impurity content can be determined based on the precipitation temperature in the plugging-meter, given the known relationship between solubility limits and temperature.

By action of the CT, the concentration of O and C are expected to be lower than the target requirement (10 wppms),

whereas H and N should be over the limits (more than 50 wppms and 1200 wppm, respectively), those requiring dedicated traps. Both N and H-traps use a gettering process (also known as hot traps), where lithium comes into contact with a reactive bed that binds non-metallic impurity elements into thermodynamically stable compounds. For the HT, Yttrium-based getter has been selected as the most suitable material given its high chemical affinity to the Hydrogen (partitioning coefficient for the yttrium-lithium-hydrogen $\approx 10^3$) [31, 32].

The efficiency of this kind of traps is strongly influenced by the working temperature, which impacts on the thermodynamics, and mass of getter. Detailed analysis of the Yttrium-Lithium-Hydrogen were made by Hendricks [33, 34]. In this context, a LL experiment, called Lithium system for Yttrium-based DEuterium Retention experiment, has been developed at the CIEMAT (Spanish Centre for Energy, Environmental and Technological Research) [35]. The experiment aims to measure critical parameters that determine hydrogen absorption capacity, enabling more extensive *in situ* validation of numerical hydrogen transport models.

In the current design, the HT works isothermically at 300 °C (reducing the risk of beryllium nitride precipitation). According to previous studies, 8–10 kg of Yttrium should be enough to reduce the Hydrogen isotopes below the limits (see table 4). Note that Hydrogen (including Tritium) is produced continuously in the Target. The Li-related tritium is mainly generated in the beam-Li interface (and additional small amounts in Li components by back-scattering within the TC). The total tritium production is calculated to be around 3.8 g per year. For safety reasons, the total tritium inventory mobilazaible in case of a plant accident must be less than 0.3 g. Therefore, during operation the tritium will be distributed 0.3 g within the Li loop and the rest will be retained in the hydrogen traps (HTs) (0.3 g each trap). To accommodate this, the design includes features that allow for monthly replacement of the traps (once filled with tritium) without interrupting the purification process. These features include double valves, quick disconnection systems, and dedicated expansion and auxiliary tanks, which facilitate the draining and filling of lithium. Those auxiliaries tanks serve also to the CT, for maintenance reasons (although no periodic replacement is foreseen).

Unlike the HT, the nitrogen strategy involves a static NT. In the current design, a vertical cylindrical tank, with a capacity to accommodate the entire lithium inventory, is equipped with 3,515 kg of titanium getter allocated inside a removable basket. Previous experiences demonstrated that titanium getter at 600 °C can reduce the concentration of N by up to a few wppms [29]. NT is sizing for the full lifetime of the facility. The trap is equipped with a dedicated electric heater and tank body is made of high temperature resistant stainless steel (AISI 347 H). This trap is connected to the DT, where the lithium is transferred after purification by support of the Argon subsystem. This process is foreseen during the initial purification of the lithium (commissioning) and during the maintenance period (when the loop is open), i.e. once per operational year.

The monitoring of the impurities in the lithium is essential for the safe operation of the ICS, ensuring that target thresholds are met and effectively controlling the efficiency and maintenance needs of the traps. A fraction of the flow is deviated towards the impurity monitoring brach (3% of ICS flow). The impurity monitoring branch is equipped with online sensors: resistivity-meter [36] and electrochemical sensor for measuring the Nitrogen and Hydrogen concentration respectively. In addition, there are two samplers for off-line analysis of the lithium and a port connection for other sensors such as the plugging-meter. Those sensors and procedures are currently under R&D.

In the near future, these monitoring and trapping technologies will be tested and validated jointly in a lithium circuit called LITEC [37], which is a Li facility with a great flexibility and a wide operational range, representative of IFMIF-DONES ICS.

4.2. Generation, distribution and deposition modeling of impurities

The evaluation of the generation and distribution of impurities in the loops is, therefore, of paramount importance for the safe operation of the facility. In order to estimate the generation and distribution of the impurities along the Li loop a numerical model has been developed. The model is continuously updated and takes into account the actual design status of the Li loop. A key input for the model is the corrosion rate of stainless steel components in contact with flowing lithium. The results of the experimental corrosion tests on the LIFUS6 facility are considered in the simulations [29, 38]. The most significant radioactive components are tritium and beryllium-7, which are considered as mobilizable elements. Therefore, particular attention is given.

4.2.1. Generation and solubility of ^{7}Be. ^{7}Be is produced in IFMIF-DONES mainly in the reactions ^{6}Li(d, n) ^{7}Be (14.5%) and ^{7}Li(d, 2n) ^{7}Be (83.1%). ^{7}Be decays to ^{7}Li with a half-life of 53.2 days by electron capture process, and it has an associated gamma emission of 477 keV. The generation of ^{7}Be has been evaluated by several studies and experimental tests dating back to the IFMIF project [39], and more recently for the IFMIF-DONES design [40]. The best estimate production rate under IFMIF-DONES operational conditions, considering natural decay (without any purification), is an equilibrium value of 150 mg in lithium, which is the reference value to monitor after one year of irradiation.

The ^{7}Be dissolved in LL in presence of nitrogen chemically reacts to form the compound Be_3N_2. Therefore, lithium solubility is evaluated considering the equilibrium of these three components by means of the following correlation [41],

$$\log_{10}\left(C_N^2 C_{SBe}^3\right) = -5.7 - 20300/T \qquad (1)$$

where C_N and C_{SBe} are the atom ratio of nitrogen and unbound beryllium in lithium, respectively. Due to the relatively high

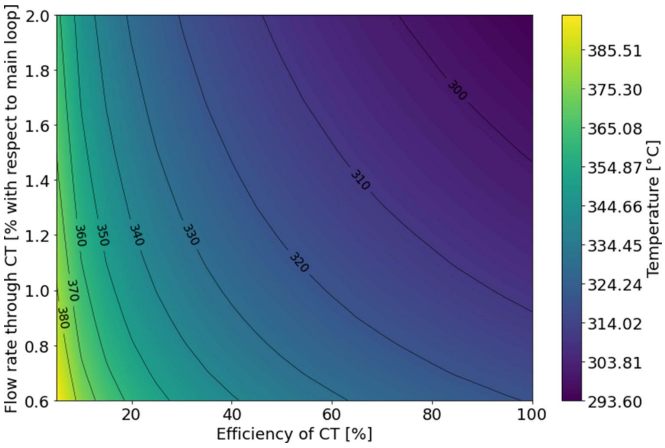

Figure 19. Saturation temperature mapping at which ^{7}Be precipitates in the Loop as Be_3N_2 as a function of CT flow rate and efficiency (for N concentration of 30 wppm).

concentration of N in the loop (see table 4), the expected content of unbound ^{7}Be should be very low theoretically (below ppb). Most of the isotope should be found in the form of Be_3N_2 which may precipitate and deposit at some locations along the loop due to the higher density than liquid Li.

4.2.2. Distribution of ^{7}Be (Be_3N_2) in the loop. According to numerical models, beryllium-7, in the form of beryllium nitride (Be_3N_2), is distributed throughout the lithium loop, with a tendency to deposit primarily in the HX1, the Cold Leg (CL) connecting HX1 to the TSY, and the CT, which is located in the ICS and operates at low temperatures. It was numerically observed that increasing both the CL temperature and flow rate in the CT positively affects the reduction of ^{7}Be deposition outside of the CT. These observations are consistent with a theoretical thermodynamic evaluation of Be_3N_2 precipitation.

Theoretical evaluations, developed for a generic system of a loop and a CT, show that the mass of Be in the Li flow is a function of trap efficiency and flow rate in the CT, for a given N concentration in the lithium. Assuming that the calculated concentrations of Be in the loop correspond to saturation values, there can be found critical operating temperatures (see figure 19). These temperatures represent the minimum levels above which the ^{7}Be concentration in the lithium would be insufficient to precipitate Be_3N_2 in the cold locations along the loop. By keeping the ^{7}Be concentration below its solubility limit at the loop temperature, Be_3N_2 will not precipitate outside the CT.

As a consequence, the results indicate that the reduction of Be deposition in the loop can be achieved by adjusting the flow rate and the operating temperature of the lithium. Changes in Li temperature and flow rate in the CT impact to the full LS design, hence a suitable selection of those parameters are essential.

On one hand, increasing the operating Li temperature significantly affects the Li loop operation, particularly by reducing the boiling margin on the Li jet surface. The boiling margin is the difference between the Li temperature and its saturation temperature at the pressure in the target vacuum chamber. This margin is maintained by the centrifugal forces of fast-flowing Li on the concave-shaped channel. The saturation temperature on the free surface is $T_s = 342.14\,^{\circ}$C at 10^{-3} Pa. Given the temperature variation of approximately 30 °C due to the beam power deposition, the Li operating temperature should not exceed 300 °C to avoid 'superficial boiling' and strong surface evaporation. Higher Li temperatures also increase the evaporation rate. However, numerical simulation has shown that the evaporated lithium is confined and deposited in the vacuum chamber and is not spread in the beam ducts.

On the other hand, the increase of lithium temperature provides a larger logarithmic mean temperature difference between Li and oil in the primary HX1 system. This larger temperature difference allows for a smaller HX1 design, which reduces the generation of corrosion products.

Regarding the flow rate through the CT, it impacts directly in the total trap capacity and heat interchanging system, although it does not suppose a technological challenge.

Considering both, the thermodynamic limits for precipitations of Be and the impact on the loop design, the bounding operating limits were defined as follows:

- Operating temperature of the lithium (cold leg) 300 °C.
- Nitrogen concentration in the lithium 30 wppm.
- Flow rate in the ICS (and so in the three CT) 2% of the main flow.

Assuming an efficiency of the CT about 80% with a flow rate of 2% (respect to main flow), the saturation temperature is lower than 300 °C. This means that no precipitation is expected in the Lithium loop (nominal temperature is 300 °C), and the ^{7}Be will precipitate (as Be_3N_2) only in the CT (working at 190 °C). Note that the efficiency of the CT is in function of the residence time through it. The design of the CT has been made to ensure a given residence time.

4.3. Impurity control strategy and safety related measures

Most of the impurities in IFMIF-DONES are confined in the traps (≈90%). In case of a severe accident in the facility, the main contribution to the mobilization of radioactive inventory is associated with the impurities dissolved in the LL, those are mainly ^{7}Be and Tritium, whilst ACPs have a low impact due to low volatility. Several reference accidental scenarios have been identified in the IFMIF-DONES safety analysis report [19] related to the partial or total release as a consequence of lithium leakage and potential fire. A defense-in-depth philosophy has been implemented in IFMIF-DONES, which involves a series of measures such as inertization of lithium rooms with argon; dynamic confinement, enclosure of the Li rooms by a leak tight stainless steel liner and installation of lithium recovery system for collecting the leakages among main ones. Reader is referred to [6] for more information about IFMIF-DONES Li fire protection system.

For strategical reasons, even when the probability of lithium fire is very low, lower than 10^{-6} yr^{-1}, design extension

conditions have been considered to the LS and traps in particular, limiting the consequences in case of a catastrophic event where all the mitigation measures fail. Under this scenario, known as Beyond Design Accident Scenario (BDAS), a dose objective of 50 mSV to the most exposed individual has been preliminary defined, but still under discussion (note that this objective value is very conservative, this being significantly lower than 250 mSv exposure tolerable by Spanish regulation for Nuclear Power Plants, Category IV, for Design Basis Accident [42]). This practically translates to limit the amount of possible release of tritium and ^{7}Be to 0.3 g and 1.2 mg, respectively. Regarding the design of the ICS, this strategy affects to the design, operation and maintenance plan of the HT and CT.

The current design of the CT system involves three trap units operating in parallel. This configuration is chosen to ensure the operating conditions that minimize ^{7}Be deposition in the main Li loop. With all three CT tanks functioning simultaneously, theoretical calculations indicate no deposition of ^{7}Be in the Li loop, as above-mentioned. Therefore, a maximum load of 50 mg per CT unit can be expected in nominal operation (which results on 150 mg in total). Assuming that 2% could potentially be mobilized in the form of Be_3N_2 aerosols in case of a Li fire of one unit [43], the potential release would be in the order of 1 mg for BDAS, which is below the conservative guideline of 1.2 mg. Therefore, as an adequate safe engineering practice, the CT units are placed in a separate room from the rest of the LS, each with a single fire sector, and isolated by safety valves. No replacement of the CTs are required from radiological point of view, though maintenance operations are take into account in the design i.e. one trap unit may be temporally stopped. Continuous monitoring of key parameters such as inertization, gamma irradiation, and tritium contamination levels are foreseen as additional safety measures.

Similar approach has been followed for HTs. Three HT units has been considered in the design, placed in a dedicated room and separate in three different sectors for fire and confinement purposes. The Tritium has a half life of 12.3 year, that would be accumulated in traps during the operation of the facility. In this case, the procedure for the HTs requires monthly replacement of each unit when loaded with 0.3 g Tritium (T), whereas the others units are available for operation. This approach provides continuous purification, even during the replacement, and increase reliability and availability.

Figure 20 shows an illustrative model of the LS layout driven by the safety impurity control strategy.

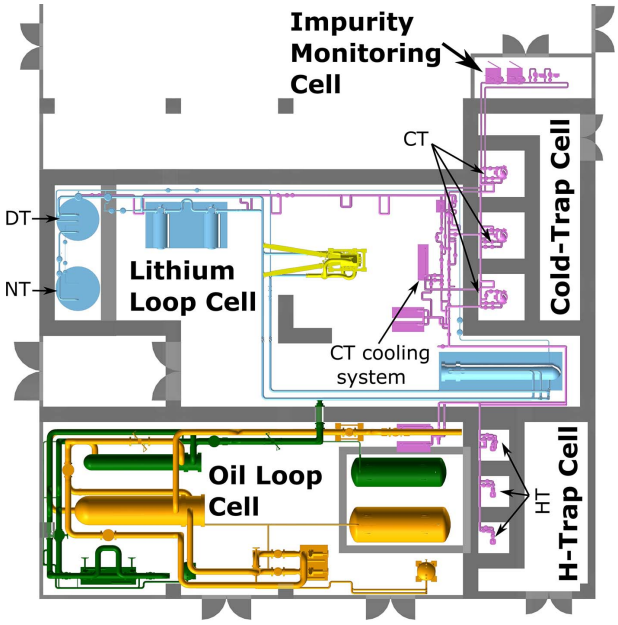

Figure 20. Layout of the Lithium Systems inside the Main Building. Lithium equipment are confined in dedicated rooms, those are: the Lithium Loop Cell, Cold-Trap Cell and H-Trap Cell. The HT and CT are divided in three units installed in separated sectors. NT is installed inside the DT pit and close by top concrete shielding.

5. Lithium diagnostics

5.1. Overview of lithium diagnostics

The LS diagnostics within the IFMIF-DONES facility are essential for ensuring the reliable and safe operation of the facility, particularly in the target area where the neutron source is generated. These diagnostics are designed to fulfill several functions: monitoring the main operational parameters of the systems (Monitoring), preventing the failure of key equipment that could impact cost and availability (Machine Protection), and protecting workers and the public from toxic or ionizing exposure and potential health risks (Safety). The design and requirements of these diagnostics aim to ensure robustness, reliability, and safety in a highly challenging operational environment.

In IFMIF-DONES the diagnostics are organized hierarchically following the plant breakdown structure. Table 5 provides an overview of main families of diagnostics for the LS.

LS diagnostic faces several key challenges. They have to withstand extremely high radiation levels, exceeding hundreds of MGy per full power year (Si-equivalent), depending on their position. Many diagnostics need to be compatible with RH methods (or hand-off) to ensure maintainability in ionized areas with limited or restricted access. Some of them are in contact with LL at high temperature, this being an aggressive element that may degrade the components. Additionally, critical diagnostics, such as the monitoring of the lithium jet thickness demands quick response times of the order of milliseconds to promptly address any deviations and ensure the smooth operation of the system. Those requirements claim the use of innovative designs and materials. Following sections provide descriptions and R&D status of main critical diagnostics.

5.2. Li jet diagnostic

One of the most important parameters to be controlled in the TSY is the thickness of the Li jet. The film thickness in the beam footprint area of the LL target has to be 25 $\pm$ 1 mm. This

Table 5. Main diagnostics families for the Lithium System (up to level III).

TSY	PLO	SLO/TLO	ICS
TSY Power	PLO Power	SLO/TLO Power	ICS Power
TSY Temperature	PLO Temperature	SLO/TLO Temperature	ICS Temperature
Target Vacuum Chamber Pressure	PLO Li Flow	SLO/TLO Li Flow	ICS Li Flow
Lithium Jet Thickness	PLO Li Pressure	SLO/TLO Li Pressure	ICS Li Pressure
Beam Position and Footprint	Primary Dump Tank Diags.	SLO/TLO Dump Tank Diags.	ICS EMP Diags.
Target Assembly Position	EMP Diags.	SLO/TLO Expansion Tank Diags.	ICS Expansion Tanks Diags.
QT Diags.	HX1 Li-Oil Diags	SLO/TLO Pump Diags.	CT Cooling System Diags.
Maintenance & Predictive Diags.	Maintenance & Predictive Diags.	HX2-3 Oil Diags.	CT Diags.
		Valve Diags	HT Diags.
		Maintenance Predictive Diags.	HT Diags.
			IMO Hydrogen Sensor
			IMO Resistivity meter
			IMO Plugging meter
			Valve Diags
			Maintenance & Predictive Diags.

requirement is set to ensure a stable neutron flux production, simultaneously contain the heat release in the LL and avoid damaging the backplate.

Previous studies have demonstrated that the lithium jet maintains a high level of stability and thickness homogeneity over time [11, 44–46]. Fast wave fluctuations have been observed on the free surface due to the turbulent regimen of the lithium jet. The average wave amplitude is about 0.26 mm (at a lithium velocity of 15 m s^{-1}) and fluctuates in milliseconds time scale (and faster depending on wave amplitude) [44]. The surface waves is then in the tolerance values and their effect on the time averaged jet thickness is zero, hence those fluctuations may not suppose an issue. However, potential defects or degradation on the surface of the nozzle exit could generate stationary waves that propagate along the jet. Measurements in a water flow facility with a concave open channel flow showed possible profiles of critical wake amplitudes [47]. These phenomena shall be carefully monitored and controlled to prevent damage to the backplate (BP), where most of the beam power is deposited within the first 22 mm of the lithium jet thickness.

Therefore, monitoring the fluid dynamic stability of the lithium jet during operation involves two types of measurements: one for jet thickness and another for monitoring the evolution of stationary waves on the jet surface. Monitoring jet thickness is crucial for safety, requiring millisecond-level measurement times and depth accuracy better than 0.5 mm. Only a few measurement points along the jet span are needed for this purpose. In contrast, monitoring stationary waves requires a significantly higher number of measurement points along the jet span, with a measurement pitch of approximately 0.5–1 mm, over a period of seconds, and with similar depth resolution.

Additionally, the extremely high radiation levels in the TC during operation (exceeding 100 MGy/fpy Si-equivalent) must be taken into account when selecting measurement systems.

Several technologies have been investigated, such as: Optical Comb Absolute Distance Meter [44]and Laser Interferometry (Lidar). An alternative based on millimeter-wave radar techniques is currently under investigation and validation, known as LiRADAR [48]. An overview of such technologies can be found in [49].

Currently, the most mature technology found that fulfills the previous listed requirements is the Laser Interferometry ITER in-Vessel Viewing System (IVVS), developed by Fusion For Energy for ITER project [50]. This system measures the intensity and phase shift of the reflected signal, using the phase shift to calculate distance [51]. It is optimized for distances between 0.5 and 10 meters and it is Radiation-Hard resistant. The optical head is separated from the laser source and detector, which are connected via an optical fiber up to 200 meters long. The main characteristics of IVVS are [52]:

- Accuracy 0.3–0.5 mm @ 1–15 m
- Spatial resolution 0.5 mm @ 5 m
- Measuring distance 0.5–10.5 m
- Radhard (total dose 10 MGy)

For the IFMIF-DONES application, the device is proposed to be installed in the Target Interface Room, located upstream of the TC, at a distance of 8–10 meters from the target. The device's head can be inserted through the secondary beam duct and shielded, which helps to reduce the irradiation dose. The system can achieve a sampling frequency above the kHz range,

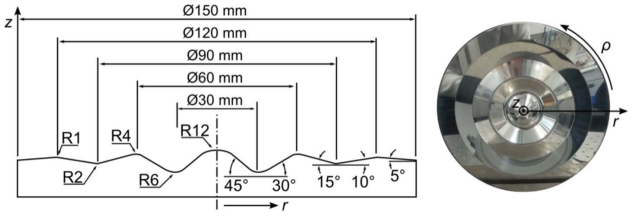

Figure 21. Solid Target for Li diagnostic test: cross-section of the surface of the solid model.

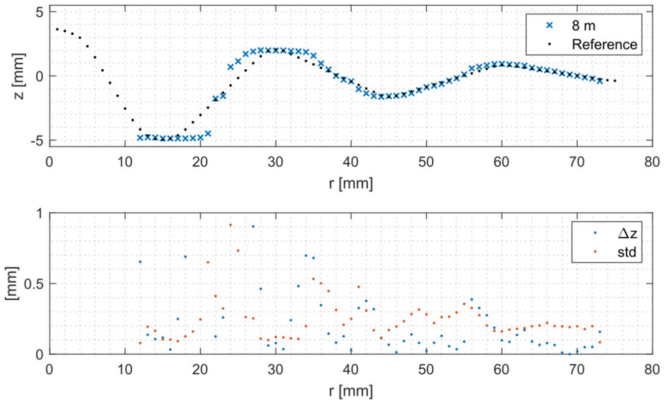

Figure 22. Top: height profile (blue crosses) of the solid model measured from 8 m distance in comparison to the given reference surface (black dots). Bottom: Deviation $\triangle z$ to the provided model and standard deviation of the points in each 2 mm window. The z-values were evaluated every millimeter using a 5% trimmed mean.

although it relies on small surface waves on the lithium jet to reflect the signal back to the sensor that is under validation.

The IVVS has been tested on two different model surfaces: a solid wavy target and a liquid metal free surface. The first consisted of an aluminum block with rings of different slopes on the surface [53]. The aim of the model surface was to measure specular slopes of different inclination from 5° to 45° and their respective minima and maxima (see figure 21).

Figure 22 shows the resulting height profiles (blue crosses) measured from an 8-meter distance, compared to the reference profile (black dots). The plot also displays the deviation from the reference model ($\triangle z$) and the standard deviation within each 2 mm window. The system successfully resolved the two outermost slopes at all measured distances, with the standard deviation increasing slightly at larger distances but remaining below 0.4 mm. Resolving the minima of a potential wake depends also on the diameter of the laser spot on the surface. In previous case the measured laser spot diameter was 3.8 mm at 8 m distance (whilst 2 mm at 4.5 m distance).

The second model surface consisted of a box with liquid GaInSn. The box was equipped with a vibration motor used to induce small surface waves, figure 23. The measurements showed that small surface waves enable the distance measurement to the specular surface. The vertical resolution is less than the required 0.3 mm. Looking at the measurement speed, scanning the width of the beam footprint required less than

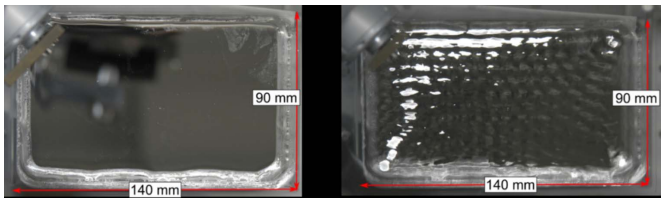

Figure 23. Box with liquid GaInSn for Li diagnostics test: Flat and wavy surface.

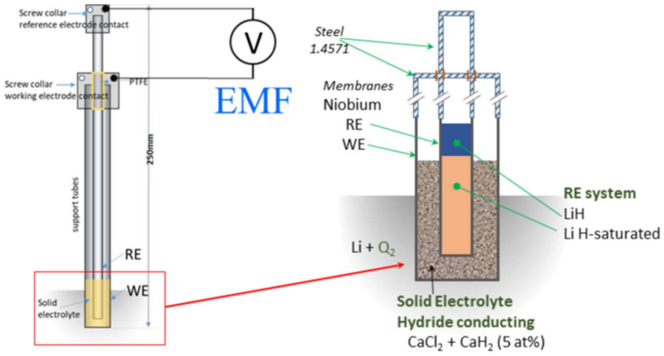

Figure 24. ECHSLL measuring principle, defining Working Electrode WE and Reference Electrode RE, and a Voltage V as result of H-concentration in the LL. Reproduced from [58]. CC BY 4.0.

100 ms. The results of the test measurements are promising for the application of the IVVS in IFMIF-DONES. Additionally, an experimental campaign on a flowing lithium jet along a DONES-like curved channel is planned for the next years.

5.3. Hydrogen diagnostic

The chemical reactivity of the LL with structural materials (tubes, tanks, pumps, etc) is increased by non-metallic impurities; also materials that are otherwise stable in lithium lose this stability especially in the presence of hydrogen and its isotopes [54], which induce danger of fatal failures under operation by embrittlement and fatigue stresses. Knowledge of their concentrations and enrichment is therefore essential. The hydrogen measurement will take place in the ICS by an Electrochemical Sensor for the Lithium Loop (ECHSLL) developed at KIT (Karlsruhe Institute of Technology) [55, 56]. The principle of operations are shown in figure 24. Sensor geometries and sizes are optimized to laboratory thermomechanical requirements under inert atmospheres (Glovebox) and to further experimental conditions of the foreseen ICS sites (flanges, spaces, connections, maintenance). In its current design, the sensor has 250 mm total length; the cylindrical potential detection part is of 14 mm diameter and 40 mm high (welded to the steel support tubes contact sites), figure 25.

Different tests were carried out under several operating conditions and using different materials [57]. The most recent tests focused on LL temperatures of 300 °C (nominal IFMIF-DONES temperature) with specific amount of added LiH (at

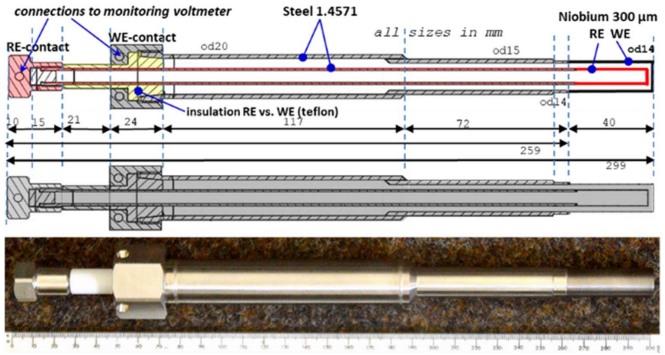

Figure 25. Recent design of ECHSLL electrode geometries and dimensions.

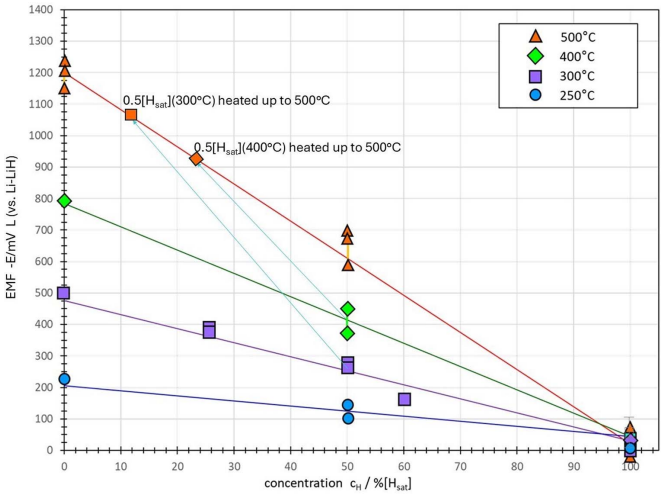

Figure 26. EMF voltage as function of [Hdiss] for Li-melts at different temperatures. Highlighted by the blue arrows are the two different concentrations 50%[Hsat] for 300 °C and 400 °C, each heated up to 500 °C. Reprinted from [56], Copyright (2022), with permission from Elsevier.

which the hydrogen solubility is 0.344 at-%). The Nb-systems showed stability for long-time measurements, in the range of some weeks. Further tests, reaching temperatures up to 500 °C confirmed the chemical stability of the system even under more extreme conditions. In figure 26 the potential measured as function of hydrogen concentrations and temperatures is reported [58]. The tests performed showed that the sensors worked properly and indicated Electromotive Force (EMF) values in good accordance with the adjusted hydrogen concentrations also in the range of some hundreds of hours. A triple-stand test is being operated and is controlled by a modern contemporary online monitoring system that enables remote control. For application in the DONES test site, reduction of the EC electrode sizes was carried out (diameters reduced to 14 mm). Furthermore, ECHSLL with drastically thinner membranes (0.3 mm) and smaller diameters are currently being manufactured in order to achieve quicker response times under operation.

6. Conclusions

This paper has shown the current design and R&D status of the IFMIF-DONES LSs, with a detailed view of the four subsystems: the TSY, the HRL, the ICS and the LSA.

The development of the TSY, devoted to generate the lithium target for the deuteron beam, entails a series of challenges due to extreme working conditions, handling high thermal loads (5–10 MW) and working under high vacuum and high irradiation environment. The target design is based on a high-speed liquid lithium jet flowing through a concave Back-Plate, efficiently removing thermal power and preventing boiling and cavitation. This concept has been proven in representative conditions with a 1:2.6 scale prototype in the IFMIF-EVEDA phase. The design of the Quench Tank has been optimized for reducing flow fluctuations and vibrations. Removable target strategy has been further developed, paying special attention to RH interfaces and including a series of novel features that allow the replacement and alignment of the Target Assembly, sensors and connectors effectively.

The HRL, responsible for transferring thermal power from the lithium to the conventional HRS, has undergone major updates. These updates involve optimizing the heat exchangers to account for the modified lithium working conditions and updating the layout to enhance the maintainability strategy. Intense effort has been dedicated to the design and characterization of the main electromagnetic pump (based on permanent magnets), capable of supplying 100 $l s^{-1}$ under nominal conditions to the target. The design includes a flywheel feature aimed at ensuring the survival of the lithium layer in the target in the event of pump trips for safety reasons.

The ICS, devoted to the purification of the lithium, plays a pivotal role in the safe and reliable operation of the Lithium Loops. A series of analyses has focused on the generation and distribution of impurities, with special emphasis on tritium and ^{7}Be. Controlling ^{7}Be is of paramount importance for radiological reasons. As shown in this paper, a suitable selection of the lithium working temperature, control of the nitrogen concentration in the lithium, and the flow rate through CT should theoretically prevent or reduce ^{7}Be precipitation along the loop outside the CT. Three CT units have been implemented, working in parallel and designed for the full life of the facility. Similarly, the ICS is equipped with three HT units, which are replaced regularly once filled with tritium. The traps are installed in dedicated rooms, physically separated into sectors for fire and confinement purposes. This strategy ensures the safe and reliable operation of the LS and controls the mobilizable radiological inventory.

An overview of lithium diagnostics is also provided, highlighting the importance of the lithium jet diagnostic. A key sensor for monitoring the lithium jet thickness in the target is the In-Vessel Viewing System, initially developed for ITER. It has been demonstrated to be a suitable technology for IFMIF-DONES, although further validation campaigns are being carried out to increase the Technology Readiness Level.

Moreover, the status of the design of a new online electrochemical sensor for the detection of hydrogen isotopes in lithium is illustrated.

Acknowledgments

This work has been carried out within the framework of the EUROfusion Consortium, funded by the European Union via the Euratom Research and Training Programme (Grant Agreement No 101052200 — EUROfusion). Views and opinions expressed are however those of the author(s) only and do not necessarily reflect those of the European Union or the European Commission. Neither the European Union nor the European Commission can be held responsible for them.

ORCID iDs

F.S. Nitti https://orcid.org/0000-0002-5176-4559
J. Maestre https://orcid.org/0000-0002-0980-7367

References

[1] Ibarra A. *et al* 2018 The IFMIF-DONES project: preliminary engineering design *Nucl. Fusion* **58** 105002
[2] Królas W. *et al* 2021 The IFMIF-DONES fusion oriented neutron source: evolution of the design *Nucl. Fusion* **61** 125002
[3] Bernardi D. *et al* 2022 The IFMIF-DONES project: design status and main achievements within the EUROfusion FP8 work programme *J. Fusion Energy* **41** 24
[4] Rueda J.J., Dongiovanni D.N., Pinna T., Torregrosa-Martin C., Ibarra A., Maestre J. and Nitti F.S. 2023 RAMI analysis of DONES lithium systems updated to the last design modifications *Fusion Eng. Des.* **193** 113792
[5] D'Ovidio G. *et al* 2024 The LiFIRE experimental facility: final design, construction and experimental campaign *Fusion Eng. Des.* **201** 114244
[6] D'Ovidio G., Martín-Fuertes F., Marugán J.C., Bermejo S. and Nitti F.S.S. 2023 Lithium fire protection design approach in IFMIF-DONES facility *Fusion Eng. Des.* **189** 113446
[7] Nitti F.S. 2010 Termofluidodinamica di un getto di Litio *PhD Thesis* Bologna University (available at: https://amsdottorato.unibo.it/2793/)
[8] Arena P., Bernardi D., Bongiovì G., Di Maio P.A., Miccichè G. and Nitti F.S. 2021 Determination of a pre-heating sequence for the DONES target assembly *Fusion Eng. Des.* **168** 112394
[9] Bernardi D., Agostini P., Miccichè G., Nitti F.S. and Tincani A. 2011 Improvement of IFMIF/EVEDA bayonet concept back-plate design *Fusion Eng. Des.* **86** 708–11
[10] Knaster J. *et al* 2015 The accomplishment of the engineering design activities of IFMIF/EVEDA: the European–Japanese project towards a Li(d,xn) fusion relevant neutron source *Nucl. Fusion* **55** 086003
[11] Kondo H., Kanemura T., Furukawa T., Hirakawa Y., Wakai E., Groeschel F., Nitti F. and Knaster J. 2015 Validation of IFMIF liquid Li target for IFMIF/EVEDA project *Fusion Eng. Des.* **96** 117–22
[12] Gordeev S., Arbeiter F., Hering W., Nitti F.S. and Schwab F. 2018 Analyses of the quench tank configuration for DONES liquid-lithium target system *Fusion Eng. Des.* **136** 330–4
[13] Gordeev S., Arena P., Bernardi D., Di Maio P.A. and Nitti F.S. 2020 Analytical and numerical assessment of thermally induced pressure waves in the IFMIF-DONES liquid-lithium target *IEEE Trans. Plasma Sci.* **48** 1485–8
[14] Arena P., Bernardi D., Bongiovì G., Di Maio P.A., Miccichè G., Nitti F.S. and Richiusa M.L. 2018 Thermomechanical analysis supporting the preliminary engineering design of DONES target assembly *Fusion Eng. Des.* **136** 1332–6
[15] Bernardi D. *et al* 2019 Towards the EU fusion-oriented neutron source: the preliminary engineering design of IFMIF-DONES *Fusion Eng. Des.* **146** 261–8
[16] Arranz F. *et al* 2024 Alignment strategy for IFMIF-DONES facility *Fusion Eng. Des.* **200** 114181
[17] Dezsi T., Nitti F.S., Tóth M., Pásti S., Balogh B. and Ibarra A. 2019 Overview of the current status of IFMIF-DONES secondary heat removal system design *Fusion Eng. Des.* **146** 430–2
[18] TEMA 2007 *Standards of the Tubular Exchanger Manufactures Association* 9th edn (TEMA)
[19] Martín-Fuertes F. *et al* 2019 Integration of safety in IFMIF-DONES design *Safety* **5** 74
[20] Voldek A.I. 1974 Induction magnetohydrodynamic machines with a liquid metal working body (available at: https://api.semanticscholar.org/CorpusID:230156991)
[21] Trainer M. 2006 Albert Einstein's patent *World Pat. Inf.* **28** 159–65
[22] Bucenieks I.E. 2003 High pressure and high flowrate induction pumps with permanent magnets *Magnetohydrodynamics* **39** 411–7
[23] Brēķis A., Buligins L., Bucenieks I., Goldteins L., Kravalis K., Lācis A., Mikanovskis O. and Jēkabsons N. 2023 Electromagnetic pump with rotating permanent magnets operation at low inlet pressures *Fusion Eng. Des.* **194** 113919
[24] Bucenieks I., Platacis E., Mikanovskis O., Zik A. and Mehta V. 2017 Helical type EM induction pump with permanently magnetized rotor for high pressure heads *Magnetohydrodynamics* **53** 423–8
[25] Bruggeman W.H. 1956 Purity control in sodium-cooled reactor systems *AIChE J.* **2** 153–6
[26] Grundy B.R. 1976 Experimental characterization of sodium cold traps and modeling of their behavior *Proc. Int. Conf. on Liq. Met. Tech. in En. Prod., Champion* (*Champion, Pennsylvania, USA, 3–6 May 1976*) (available at: https://inis.iaea.org/records/7n169-s9122)
[27] Hinze R.B. 1970 Chemical Engineering Progress *Symp. Series: Nuclear Engineering Part XXI* vol 66 pp 94–106 (available at: https://archive.org/details/sim_chemical-engineering-progress_1970_66_index)
[28] Osterhout M.M. 1978 Control of oxygen, hydrogen, and tritium in sodium systems at Experimental Breeder Reactor II *Technical Report* (Argonne National Laboratory) (https://doi.org/10.2172/5750291)
[29] Aiello A., Tincani A., Favuzza P., Nitti F.S., Sansone L., Miccichè G., Muzzarelli M., Fasano G. and Agostini P. 2013 Lifus (lithium for fusion) 6 loop design and construction *Fusion Eng. Des.* **88** 769–73
[30] Mangus D., Napora A., Briggs S., Anderson M. and Nollet W. 2021 Design and demonstration of a laboratory-scale oxygen controlled liquid sodium facility *Nucl. Eng. Des.* **378** 111093
[31] Smith F.J., Land J.F., Begun G.M. and de Batistoni A.M.L.G. 1979 The solubility and isotopic exchange equilibrium for hydrogen isotopes in lithium *J. Inorg. Nucl. Chem.* **41** 1001–9
[32] Begun G.M., Land J.F. and Bell J.T. 1980 High temperature equilibrium measurements of the yttrium–hydrogen isotope (H_2, D_2, T_2) systems *J. Chem. Phys.* **72** 2959–66
[33] Hendricks S.J., Carella E., Moreno C. and Molla J. 2020 Numerical investigation of hydrogen isotope retention by an

yttrium pebble-bed from flowing liquid lithium *Nucl. Fusion* **60** 106017
[34] Hendricks S.J., Molla J., Urgorri F.R. and Carella E. 2023 Impact of yttrium hydride formation on multi-isotopic hydrogen retention by a getter trap for the DONES lithium loop *Nucl. Fusion* **63** 056012
[35] Hendricks S.J. 2023 Modeling and experimental design to characterize permeation and gettering of hydrogen isotopes in fusion materials *PhD Thesis* Universidad Carlos III de Madrid (available at: https://info.fusion.ciemat.es/PhDThesis/Hendricks.pdf)
[36] Marinari R., Favuzza P., Bernardi D., Nitti F.S. and Di Piazza I. 2021 CFD optimization of the resistivity meter for the IFMIF-DONES facility *Energies* **14** 2543
[37] Garcinuño B., García A., Sánchez-Arenillas M. and Rapisarda D. 2024 LITEC: an experimental facility for the validation of the IFMIF-DONES impurity control system *Fusion Eng. Des.* **201** 114283
[38] Favuzza P. *et al* 2018 Erosion-corrosion resistance of reduced activation ferritic-martensitic steels exposed to flowing liquid lithium *Fusion Eng. Des.* **136** 1417–21
[39] Simakov S.P., Fischer U. and Von Möllendorff U. 2004 Assessment of the 3H and 7Be generation in the IFMIF lithium loop *J. Nucl. Mater.* **329** 213–7
[40] Frisoni M., Bernardi D. and Nitti F.S. 2020 Nuclear assessment of the IFMIF-DONES lithium target system *Fusion Eng. Des.* **157** 111658
[41] Ida M., Nakamura H. and Sugimoto M. 2007 Estimation and control of beryllium-7 behavior in liquid lithium loop of IFMIF *Fusion Eng. Des.* **82** 2490–6
[42] de Seguridad Nuclear C. 2015 *Instrucción IS-37. Sobre anáLisis de Accidentes Base de Diseño en Centrales Nucleares. BOE núm. 49* (BOE) (available at: www.boe.es/eli/es/ins/2015/01/21/is37)
[43] Jeppson D.W. 1982 Scoping studies: behavior and control of lithium and lithium aerosols *Technical Report* (Hanford Engineering Development Laboratory) (https://doi.org/10.2172/5182052)
[44] Kanemura T., Kondo H., Furukawa T., Hirakawa Y., Hoashi E., Yoshihashi S., Horiike H. and Wakai E. 2015 Measurement of Li target thickness in the EVEDA Li test loop *Fusion Eng. Des.* **98** 1991–7
[45] Kondo H., Kanemura T., Yamaoka N., Miyamoto S., Ida M., Nakamura H., Matushita I., Muroga T. and Horiike H. 2007 Measurement of free surface of liquid metal lithium JET for IFMIF target *Fusion Eng. Des.* **82** 2483–9
[46] Kanemura T., Sugiura H., Yamaoka N., Yoshihashi-Suzuki S., Kondo H., Ida M., Matsushita I. and Horiike H. 2011 Wave period of free-surface waves on high-speed liquid lithium JET for IFMIF target *Fusion Eng. Des.* **86** 2462–5
[47] Brenneis B., Gordeev S., Ruck S., Stoppel L. and Hering W. 2021 Wake shape and height profile measurements in a concave open channel flow regarding the target in DONES *Energies* **14** 6506
[48] de la Morena C. *et al* 2023 Assessment of a millimeter-wave radar system for real-time diagnosis of the IFMIF-DONES lithium target *15th Int. Symp. Fusion Nuclear Technology (ISFNT-15)* (*Las Palmas de Gran Canaria, Spain*) pp 11–15 (available at: https://isfnt2023.com/)
[49] Torregrosa-Martin C. *et al* 2023 Overview of IFMIF-DONES diagnostics: requirements and techniques *Fusion Eng. Des.* **191** 113556
[50] Neri C., Bartolini L., Coletti A., de Collibus M.F., Fornetti G., Pollastrone F., Riva M. and Semeraro L. 2007 The laser in vessel viewing system (IVVS) for ITER: test results on first wall and divertor samples and new developments *Fusion Eng. Des.* **82** 2021–8
[51] Siegel T. *et al* 2019 In-vessel viewing system prototype performance measurements and simulation of measurement quality across the ITER in-vessel components *Fusion Eng. Des.* **146** 2348–52
[52] Neri C., Costa P., De Collibus M.F., Florean M., Mugnaini G., Pillon M., Pollastrone F. and Rossi P. 2011 ITER in vessel viewing system design and assessment activities *Fusion Eng. Des.* **86** 1954–7
[53] Hillenbrand M.P. 2008 *Qualifizierung Einer Messtechnik zur Erfassung Freier Grenzflächen bei Flüssigmetallen* vol 7437 (FZKA) (available at: www.semanticscholar.org/paper/Qualifizierung-einer-Messtechnik-zur-Erfassung-bei-Hillenbrand/7f9878b57719e7acfdc16c41b398dd6531ef864e)
[54] Maroni V.A. 1973 A review of the chemical, physical, and thermal properties of lithium that are related to its use in fusion reactors *Technical Report* (Argonne National Laboratory) (https://doi.org/10.2172/4546804)
[55] Holstein N., Krauss W., Konys J. and Nitti F.S. 2019 Development of an electrochemical sensor for hydrogen detection in liquid lithium for IFMIF-DONES *Fusion Eng. Des.* **146** 1441–5
[56] Holstein N., Krauss W. and Nitti F.S. 2022 Detection of hydrogen as impurity in liquid lithium: an electrochemical hydrogen-sensor for IFMIF-DONES *Fusion Eng. Des.* **178** 113085
[57] Holstein N., Krauss W. and Nitti F.S. 2022 Electrochemical hydrogen detection in DONES loop materials *Nucl. Mater. Energy* **31** 101192
[58] Holstein N., Krauss W. and Nitti F.S. 2023 Development and basic qualification steps towards an electrochemically based H-sensor for lithium system applications *J. Nucl. Eng.* **4** 1–10